Electronic Supplementary Information

Graphene-coated Nickel in Biological Environments: Role of Structural Defects

Ramesh Devadig[1,2,3], Pawan Sigdel[1,2,3], Md. Hasan-Ur Rahman[1,2,3], Pulickel M. Ajayan[4*], Muhammad M. Rahman[4*], Venkataramana Gadhamshetty[1,2,3*]

[1]Civil and Environmental Engineering, South Dakota Mines, 501 E. St. Joseph Street, Rapid City, SD, 57701, USA
[2]2D-materials for Biofilm Engineering, Science and Technology (2DBEST) Center, South Dakota Mines, 501 E. St. Joseph Street, Rapid City, SD, 57701, USA
[3]Data-Driven Materials Discovery for Bioengineering Innovation Center, South Dakota Mines, 501 E. St. Joseph Street, Rapid City, SD, 57701, USA
[4]Department of Materials Science and NanoEngineering, Rice University, Houston, TX 77030, USA

Contents

Section 1. Chemical vapor deposition and transfer process

Chemical vapor deposition (CVD)

Here, the bare nickel (Ni) samples were precleaned sequentially using acetone, methanol, isopropanol, and distilled water (3 mins each), respectively, and dried using nitrogen gas. These samples were introduced into the central zone of the furnace that was vented with 500 sccm argon (Ar) to achieve and maintain ≥746 Torr inside the chamber. The furnace was sealed using the end cap with O-ring. The leak tests were carried out by sucking the air from the furnace to create 30 mTorr and the pressure is checked for its stabilization for 1 min. After the leak tests were successful, the Ni foils were annealed for 30 mins using the hydrogen (H_2) flow (16 sccm) at 30 mTorr, at 1050 °C. The graphene (Gr) growth was carried out for 30 mins using H_2 (21 sccm) and methane (CH_4) (0.105 sccm) as carrier and precursor gases, respectively. The pressure inside the furnace was maintained at 250 mTorr. After the growth, the H_2 flow was maintained to 16 sccm while maintaining the furnace pressure at 250 mTorr. The furnace was then cooled naturally until the temperature (T) reached 200 °C. The furnace cover was opened to cool the furnace to the ambient conditions.

Transfer process

The process of transferring Gr onto Si/SiO_2 substrates using ferric chloride ($FeCl_3$) and polymethyl methacrylate (PMMA) included the following protocols[1]. Gr/Ni was spin-coated with PMMA at 2000 rpm and for 2 mins to obtain a uniform PMMA film. This PMMA-coated Gr/Ni surface was kept on the hot plate at 100 °C for 10 mins to evaporate the solvent and harden the PMMA film. This step ensures that the PMMA film acts as a protective layer during subsequent processes. This PMMA-coated Gr/Ni was then etched using 1M $FeCl_3$ [2] by immersing in it. $FeCl_3$ selectively etches the Ni while not affecting the PMMA or graphene. After completely etching the Ni, the PMMA/graphene film was thoroughly rinsed with DI water (three 5-minute cycles) to remove any residual etchant. The floating film was then transferred to a prepared Si/SiO_2 substrate. To enhance adhesion, the film was air-dried for 30 minutes, followed by heating at 100°C for 20 minutes. Finally, the PMMA layer was dissolved by immersing the sample in acetone for 15 minutes, leaving a pristine graphene film on the Si/SiO_2 substrate.

Section 2. Sulfate-reducing bacteria culture and 16s rRNA sequencing

SRB culture

Lactate-C media used for SRB culture comprised of the following components (g/L): sodium lactate, 6.8; ammonium chloride, 1.0; dehydrated calcium chloride, 0.06; sodium sulfate, 4.5; magnesium sulfate, 2.0; potassium phosphate monobasic, 0.5; sodium citrate, 0.3 and yeast extract)[3]. The media was sterilized in an autoclave at 121 °C for 30 min in a liquid mode. Cultures were grown in 150 mL sealed serum bottles containing 90 mL of the sterilized Lactate-C media, which was then deoxygenized by purging the pure N2 for 20 minutes. SRB cultures were grown by injecting 10 mL of inoculum into N2-purged Lactate-C media. These cultures were incubated in an orbital platform shaker with an agitation speed of 125 rpm for 48 h at 30 °C.

16s rRNA sequencing

Methods: The planktonic cells were harvested by centrifugation at 8000 rpm for 15 min. The genomic DNA was extracted using a DNA extraction kit following the manufacturer's protocol (PureLinkTM Microbiome DNA Purification Kit). Molecular characterization was performed using 16S rRNA gene amplification and gene sequencing techniques. The PCR tests were performed with 100 ng of genomic DNA template using 8F and 1492R as universal primers. The PCR conditions and the genetic homology studies were performed as reported in our previous study[4].

Results: Molecular identification by 16S rRNA gene sequencing studies revealed the purity of OA-G20 from the MIC studies. The BLAST analysis revealed that the 16S rRNA marker gene showed 98.3% identity (with a 100% query coverage) with *Oleidesulfovibrio alaskensis* G20 (Acc No: CP000112.1).

Section 3. Ni concentration measurement and sessile cell analysis

Sessile cell count

To quantify the sessile cells in biofilms formed on the Ni coupons after 24-day MIC experiments, the exposed coupons were washed with sterile distilled water (DI) to remove unattached cells. The sessile cells were then removed by swabbing the coupons with sterile cotton swabs. 10 ml of sterile distilled (DI) water was added to the swabs, and the mixture was vigorously shaken to release the attached cells and achieve a homogeneous distribution. These suspended cells were serially diluted up to 10^{-5} in DI water. Lactate-C agar plates (2%(w/v) with Lactate-C medium) were utilized for incubation at 37 °C for 48 hours to facilitate the quantification of bacterial colonies under anaerobic condition. The biofilm colonies were counted and converted to colony-forming units per square centimeter ($CFU.cm^{-2}$).

Ni concentration

Ni concentrations in the spent electrolytes were analyzed with an Agilent 7900 Inductively Coupled Plasma Mass Spectrometer (ICP-MS). 1mL of thoroughly mixed electrolyte was collected from the serum bottle reactors at the end of the corrosion tests. These samples were acidified to a 2% acid content with nitric acid (TraceMetal Grade, Fisher Chemical) and diluted 10-fold prior to analysis. The ICP-MS was operated in the helium collision mode and quantification was performed by external calibration with a multipoint calibration curve prepared by serial dilution of a multielement standard solution (28SCP-AES, SCP Science). A second multielement standard (ICP-MSCS-PE3, High Purity Standards) was analyzed to verify calibration accuracy. Scandium and germanium were added at 1 ppm concentrations from a standard blend (SCP-ICS7, SCP Science) and analyzed to correct for any matrix effects and instrumental drift. Data processing and corrections were performed using the Agilent Masshunter software (v 4.1).

Section 4. Electrochemical measurements

The electrochemical measurement used the exposure area of 1 cm^2 in abiotic and biotic tests. To ensure accurate and reliable measurements, the data were collected after achieving steady-state open circuit voltage (OCV) conditions[5]. The Linear Polarization Resistance (LPR) tests were conducted in triplicate, with the following parameters: a potential range of ±10 mV (vs. open-circuit potential (OCP)), a scan rate of 0.125 mV/s, an initial delay of 1200 s, and a stability set at 0.1 mV/s. Polarization resistance (R_p) and corrosion current ($i_{corr)}$ were determined from the LPR tests, utilizing Tafel constant values obtained from the Tafel experiment using anodic and cathodic slopes. Following this, cyclic voltammetry (CV) tests were performed through within a potential range of -200 mV to +400 mV (vs. Ag/AgCl) at a scan rate of 0.25 mV/s. Potentiodynamic polarization (PDP) tests were carried out within the potential range of ±250 mv (vs. OCP) with a scan rate of 0.2 mV/s. Electrochemical impedance spectroscopy (EIS) tests were executed at the OCP, employing an AC signal with an amplitude of ±10 mV. The corresponding EIS spectra were acquired in the frequency range of 10000 to 0.01 Hz.

In order to comprehensively evaluate the effects of the sterile Lactate-C medium, additional tests were performed by exposing the samples (bare Ni, dGr/Ni, and biGr/Ni) to sterile Lactate-C medium for 24 days in serum bottle reactors (abiotic control). These tests aimed to assess the qualitative aspects and determine the impact of the medium in the absence of OA-G20 cells. To extract the electrochemical parameters in various corrosion processes (abiotic and biotic), an equivalent electrical circuit (EEC) was employed to fit the results obtained from electrochemical impedance spectroscopy (EIS) (Figure S1i). Gamry Echem Analyst software was used to fit the EIS data. This EEC analysis used to explain the electrochemical behavior followed a two-time constant model that is connected in series with the solution resistance (R_s). The first-time constant represents pore resistance (R_{po}) which accounts for ionic or electron conductive pathways that are created on electrode surface of bare Ni or Gr coating along with any corrosion products. The constant phase element (*CPE*) (Q_{po}) describes the corresponding pore capacitance of the pores on the bare Ni or Gr surfaces that intercept the entry of aggressive electrolytes onto the Ni surface. The second-time constant is the resistance to the charge transfer (R_{ct}) which reflects the single kinetically controlled reaction between Ni and the electrolyte and the capacitance due to the double-layer phenomenon (Q_{dl})[5]. *CPE* was transformed into capacitance using the following equation.

$$C = (CPE * R)^{\frac{1}{\alpha}} / R$$

The exponent α represent the phase shift representing the degree of deviation of the *CPE* exponent from the ideal capacitive behavior[6]. The χ2 test confirms excellent goodness of fit between the measured and predicted values for the EIS data (goodness of fit = 10^{-4}, average residual <1%).

Table S1. EEC fitting results for OA-G20 exposed bare Ni, dGr/Ni and biGr/Ni for 24 days corrosion test.

Days	**Sample**	**kΩ.cm^2**		**μF.cm^{-2}**				
		R_{po}	R_{ct}	C_{po}	α_1	C_{dl}	α_2	χ^2 (10^{-3})
0	Ni	423±29	26.3±6.3	56.9±2.2	0.94	130±18	0.90	0.34
	dGr/Ni	34.0±8.1	1.35±0.28	335±13	0.79	788±94	0.76	0.35
	biGr/Ni	62.8±3.6	18.1±3.4	176±21	0.87	175±22	0.87	0.13
6	Ni	125±1.6	10.0±0.62	47.2±0.06	0.90	84.1±4.0	0.97	0.79
	dGr/Ni	88.2±2.3	10.7±1.0	77.6±1.2	0.88	103±4.2	0.95	0.73
	biGr/Ni	132±4.6	28.0±1.8	187±18	0.96	136±15	0.85	0.30
12	Ni	13.4±2.6	122±3.6	129±15	0.91	76.0±5.0	0.92	0.25
	dGr/Ni	10.1±0.9	10.4±1.9	115±24	0.89	184±21	0.87	0.40
	biGr/Ni	18.4±2.7	115±3.8	131±14	0.89	98.7±7.0	0.92	0.37
18	Ni	66.2±5.3	25.3±±3.0	99.6±9.5	0.90	43.8±9.1	0.92	1.0
	dGr/Ni	9.58±1.0	6.35±0.90	35.8±4.8	0.92	232±22	0.88	0.52
	biGr/Ni	16.5±6.4	102±9.3	140±45	0.87	133±37	0.92	0.28
24	Ni	36.8±2.6	47±3	57.8±1.9	0.88	255±32	0.99	0.56
	dGr/Ni	0.112±0.090	6.6±0.2	84.2±1.3	0.89	389±4.8	0.68	0.86
	biGr/Ni	25.2±1.0	82±2	50.8±1.3	0.9	77.1±1.9	0.94	0.84

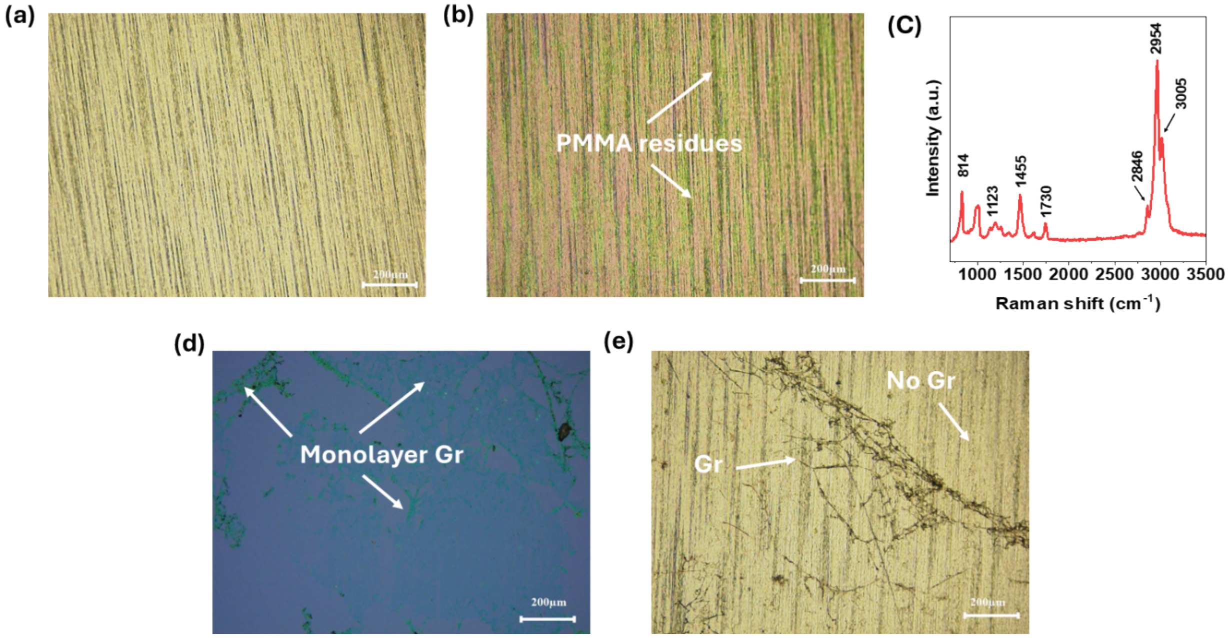

Figure S1. Optical images emphasizing the PMMA residues and discontinuous monolayer Gr. (a) Bare Ni observed through the confocal laser Scanning microcopy (b) Bare Ni coated with PMMA residues observed as greenish color in optical images (c) PMMA signatures confirmed through the Raman spectroscopy (d) Discontinuous monolayer Gr transferred on Si/SiO2 for characterization (e) Optical image highlighting the monolayer Gr on Ni.

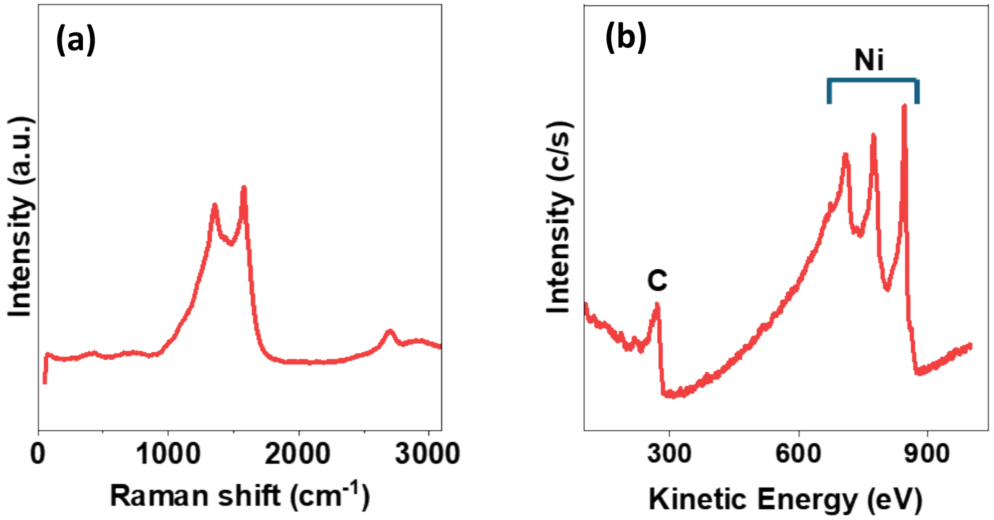

Fig. S2. Characterization of nickel carbide on dGr/Ni. (a) Raman signatures of nickel carbide showing the early incomplete graphene growth (b) Nano Auger spectroscopy confirming the spectra for nickel carbide.

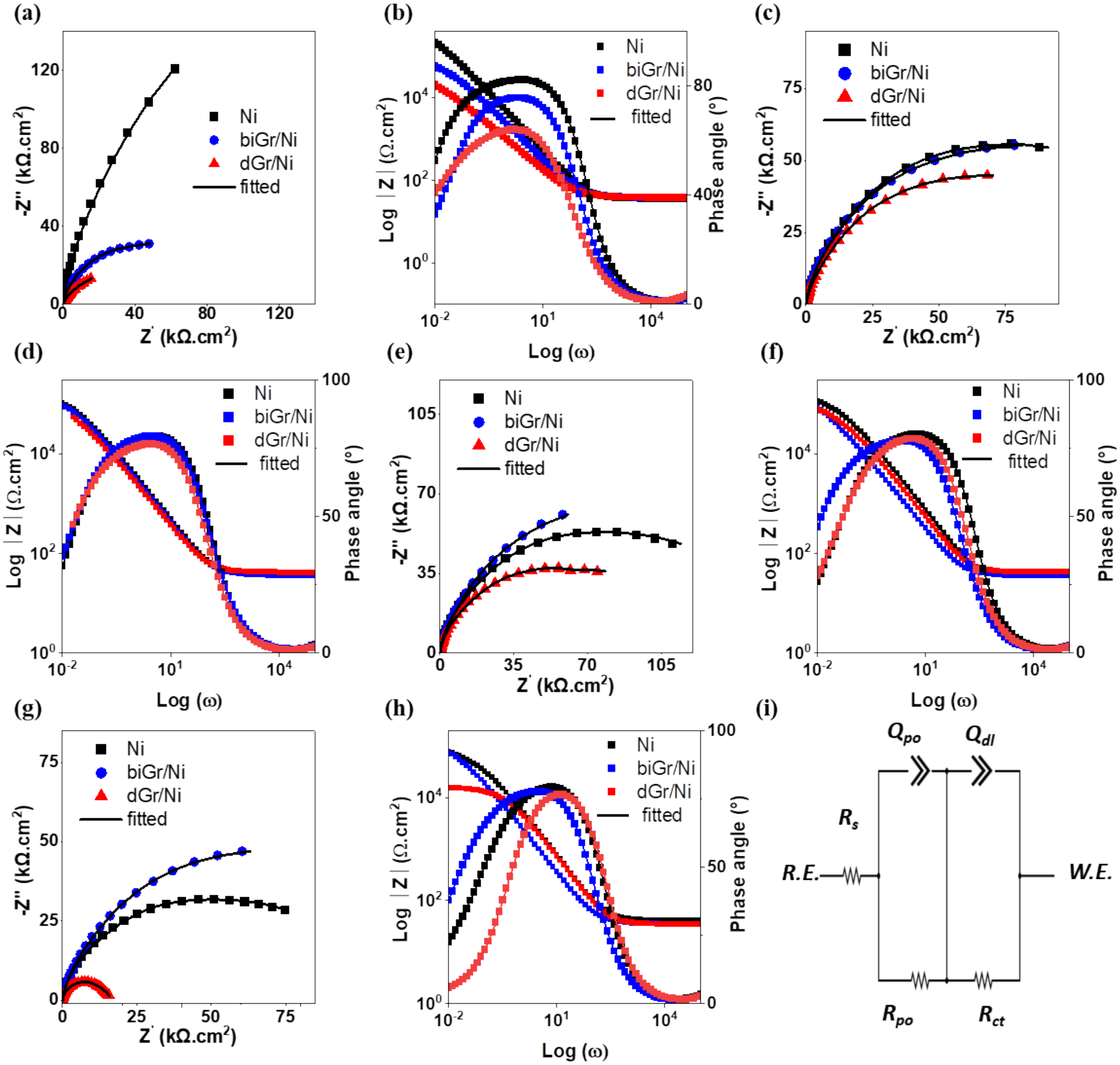

Figure S3. Microbial corrosion resistance performance of Ni, dGr/Ni, and biGr/Ni exposed to *Oleidesulfovibrio alaskensis*- G20 for 24 days. Temporal variation of (a) Nyquist plot on day-0 (b) Bode plot on day-0 (c) Nyquist plot on day-6 (d) Bode plot day-6 (e) Nyquist plot on day-12 (f) Bode plot on day-12 (g) Nyquist plot on day18 (h) Bode plot day-18 (i) Equivalent circuit used for the analysis of EIS data.

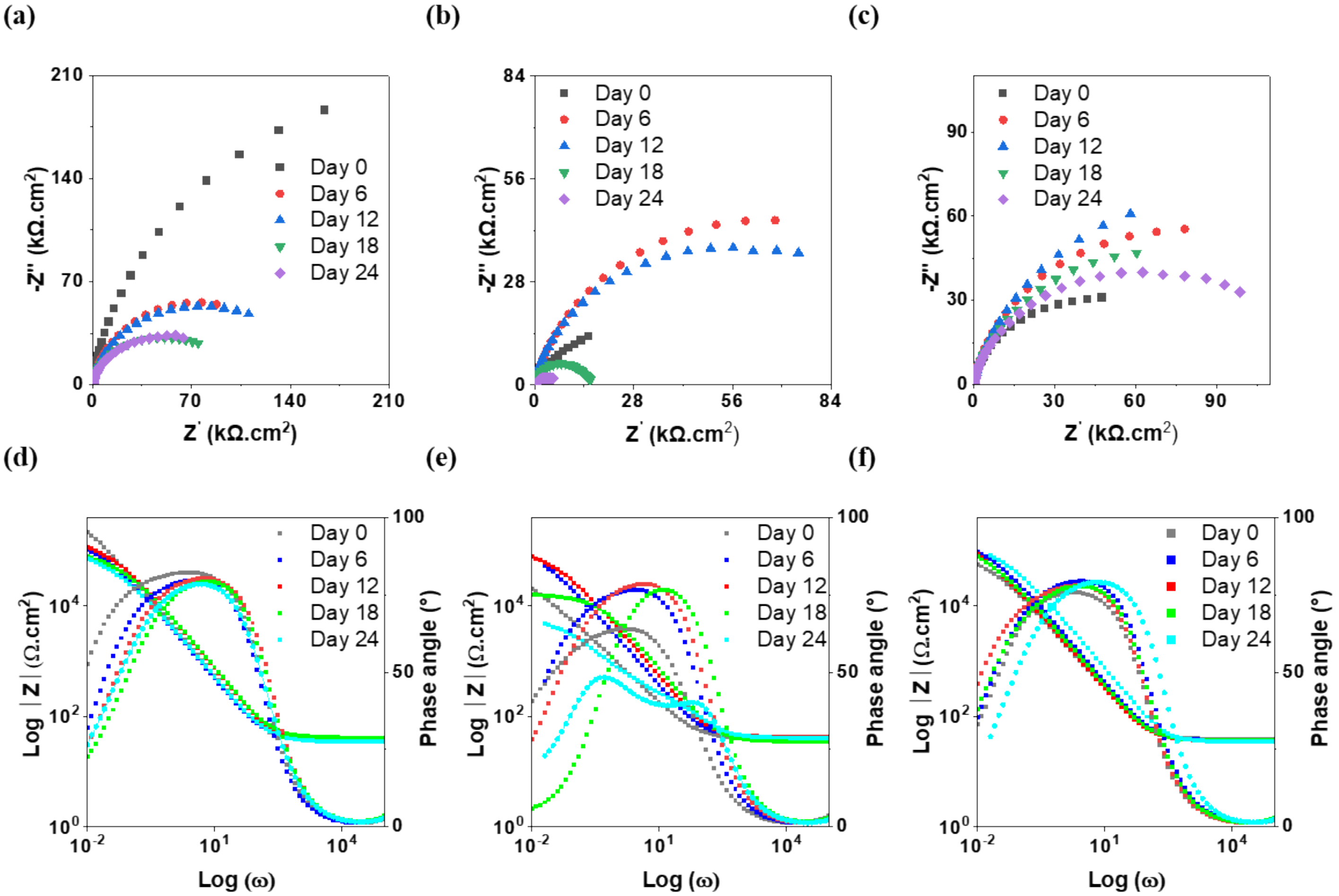

Figure S4. Temporal variation of electrochemical impedance spectra for bare Ni, dGr/Ni and biGr/Ni for 0 -24-day microbial exposure. (a) Nyquist plot for bare Ni (b) Nyquist plot for biGr/Ni (c) Nyquist plot for dGr/Ni (d) Bode plot for bare Ni (e) Bode plot for biGr/Ni (f) Bode plot for dGr/Ni

Table S2. Calculation of inhibition efficiency of the coated sample (dGr/Ni and biGr/Ni) against the bare Ni

Days	dGr/Ni (%)	Error	biGr/Ni (%)	Error
6	-37.3	7.6	10.7	4.8
12	-38.7	6.4	30.9	5.4
18	-28.2	7.9	41.3	4.9
24	-97.2	6.1	30.3	1.6

Calculation of inhibition efficiency [7,8]

$$\text{Inhibition Efficiency} = (I_{corr} - I_{\text{corr}}^{*}) / I_{\text{corr}} \times 100$$

Where I_{corr} = corrosion current in the bare Ni,
$I_{\text{corr}}*$ = corrosion current in the coated samples (biGr/Ni and dGr/Ni).

Table S3. Tafel fit for biotic test on day 24

Sample	**βa (mV/decade)**	**βc (mV/decade)**	**i_{corr} (μA)**	**E_{corr} mV**
Ni	176	221	3.4	-417
dGr/Ni	334	236	8.6	-447
biGr/Ni	694	197	1.9	8.25

Section 5. Electrochemical analysis of defect-mediated abiotic corrosion mechanisms: The findings on defect-mediated corrosion behavior of Gr/Ni in biotic environments were compared with abiotic tests using sodium sulfate (SS) and sulfuric acid (SA) electrolytes, respectively (Figure S3). The nobler open circuit voltage (OCV) for dGr/Ni in SS and SA electrolytes (-307±13 mV and -339±7 mV, respectively) were 2.5-fold and 3-fold greater than biGr/Ni (-130±4 mV and -50±2 mV, respectively) (Figure S5a). The dGr/Ni exhibited smaller impedance loop and smaller capacitive loop than biGr/Ni and bare Ni in both tests (Figure S5b, Figure S5c). The Bode magnitude ($|Z|_{0.01\ \mathrm{Hz}}$) value for dGr/Ni (50.3 kΩ.cm^2) was also lower than bare Ni (74.8 kΩ.cm^2) and biGr/Ni (133 kΩ.cm^2) exposed to the identical SS electrolytes (Figure S5e). In the SA test, the value of $|Z|_{0.01\ \mathrm{Hz}}$ for dGr/Ni further decreased to 29.0 kΩ.cm^2 compared to bare Ni (44.9 kΩ.cm^2) and biGr/Ni (69.2 kΩ.cm^2), respectively (Figure S5f).

EEC analysis (Figure S3) revealed distinct defect-mediated corrosion performances of the three systems, as noted by their R_{po} and R_{ct} values. In the SS test, dGr/Ni exhibited the least R_{po} (12±1 kΩ.cm^2) than bare Ni (35±0.3 kΩ.cm^2) and biGr/Ni (322±5 kΩ.cm^2), respectively. A similar trend was observed in the SA test, where dGr/Ni showed least R_{po} (19±0.4 kΩ.cm^2) than bare Ni (21±1 kΩ.cm^2) and biGr/Ni (132±3 kΩ.cm^2), respectively. The lower R_{po} in dGr/Ni is due to the presence of Gr islands, reactive Gr edges, and GBs, while higher R_{po} in biGr/Ni indicates the absence of these defects as well as minor influence of the cracks on the Gr performance. These observations are supported by poor R_{ct} values of dGr/Ni in both SS (17±1 kΩ.cm^2) and SA (9±1 kΩ.cm^2) tests, as opposed to bare Ni and biGr/Ni. Interestingly, biGr/Ni displayed 2-fold higher R_{ct} values than bare Ni in both the SS and SA tests (Table S4).

Polarization resistance (R_{p}) and corrosion current (i_{corr}) values obtained from linear polarization resistance (LPR) plots supported findings from the EEC analysis. The R_{p} values for dGr/Ni in both the SA (0.4±0.01 kΩ.cm^2) an SS tests (48±0.9 kΩ.cm^2) were 4-fold and 2-fold lower than bare Ni, respectively (Figure S5d). For biGr/Ni, R_p values in SA (1.4±0.02 kΩ.cm^2) and SS (259±6.5 kΩ.cm^2) tests were 2.5-fold and 2-fold higher than bare Ni, respectively, consistent with R_{ct} and R_{po} trends. Consequently, dGr/Ni experienced 2-fold and 6-fold higher i_{corr} values in SA and SS tests, respectively, while biGr/Ni displayed 2-fold lower values in both tests, suggesting 2-fold higher corrosion resistance (Figure S5i). These increased trends of i_{corr} values of dGr/Ni align with the i_{corr} obtained from Tafel pitting (Figure S5h, Figure S5i, Table S5). The dGr/Ni indicated a 9-fold increase in i_{corr} in both SA and SS tests compared to bare Ni, while biGr/Ni reduced i_{corr} by approximately 2-fold compared to bare Ni.

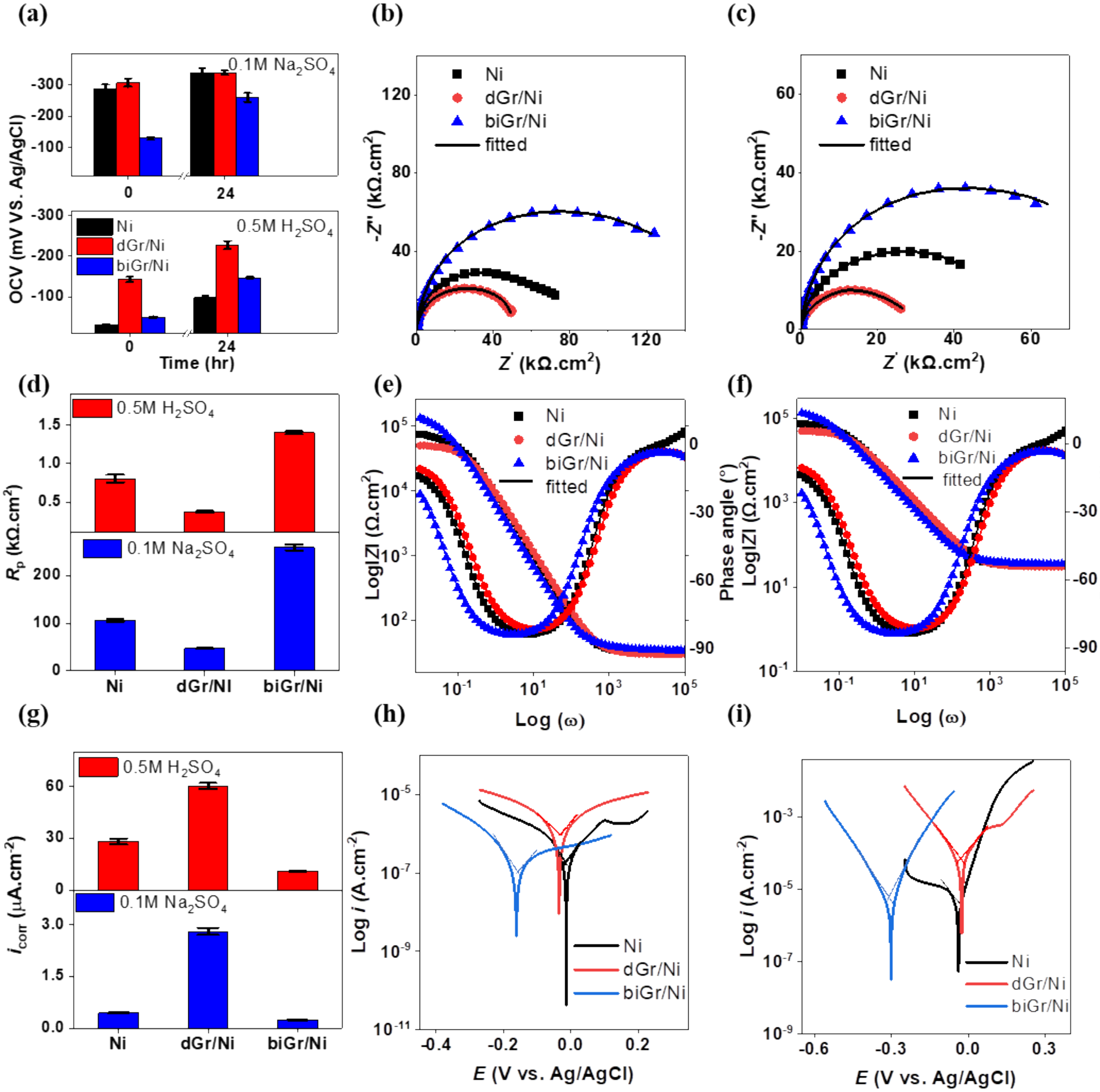

Figure S5. Electrochemical analysis of defect-mediated corrosion mechanisms under abiotic conditions. (a) Open circuit potential (OCP) profiles (b) Nyquist plot for Na_2SO_4 (c) Nyquist plot for H_2SO_4 (d) Polarization resistance (R_p) profiles (e) Bode plots for Na_2SO_4 (f) Bode plots for H_2SO_4 (g) Corrosion current (i_{corr}) profiles (h) Tafel plots for Na_2SO_4 (i) Tafel plots for H_2SO_4. Potentiodynamic polarization plots were obtained in a potential range of ± 250mV from the OCP. Electrochemical impedance spectroscopy was carried out in a frequency range of 10^5~10^{-2} Hz and amplitude of 10 mV sinusoidal disturbance.

Table S4. EEC analysis with R_{ct} and R_{po} values for abiotic corrosion resistance performance

System	Sample	kΩ.cm^2		µF.cm^{-2}				χ^2
		R_{po}	R_{ct}	C_{po}	α_1	C_{dl}	α_2	(10^{-3})
Sodium Sulfate (0.1 M)	Ni	35±0.3	84±8	91±2	0.91	616±94	0.68	1.6
	dGr/Ni	12±1	17±1	36±5	0.93	110±12	0.89	0.60
	biGr/Ni	322±5	160±11	57±9	0.77	87±3	0.98	1.3
Sulfuric Acid (0.5 M)	Ni	21±1	57±4	32±2	0.99	44±2	0.90	1.1
	dGr/Ni	19±0.4	9±1	30±1	0.90	393±43	0.99	0.83
	biGr/Ni	132±3	112±4	36±1	0.93	10±2.0	1.0	2.4

Table S5. Tafel fit details for abiotic tests

System	Sample	βa (mV/decade)	βc (mV/decade)	*i*i_{corr} (μA)	E_{corr} mV	Corrosion rate (mpy)
Sodium Sulfate (0.1 M)	Ni	257	188	0.65	-13.4	0.28
	dGr/Ni	709	541	6.2	-144	2.6
	biGr/Ni	1451	155	0.40	-75.9	0.17
Sulfuric Acid (0.5 M)	Ni	61.2	348	7.1	-38.0	3.0
	dGr/Ni	101	107	64	-335	27
	biGr/Ni	59.2	86.6	3.9	-243	1.7

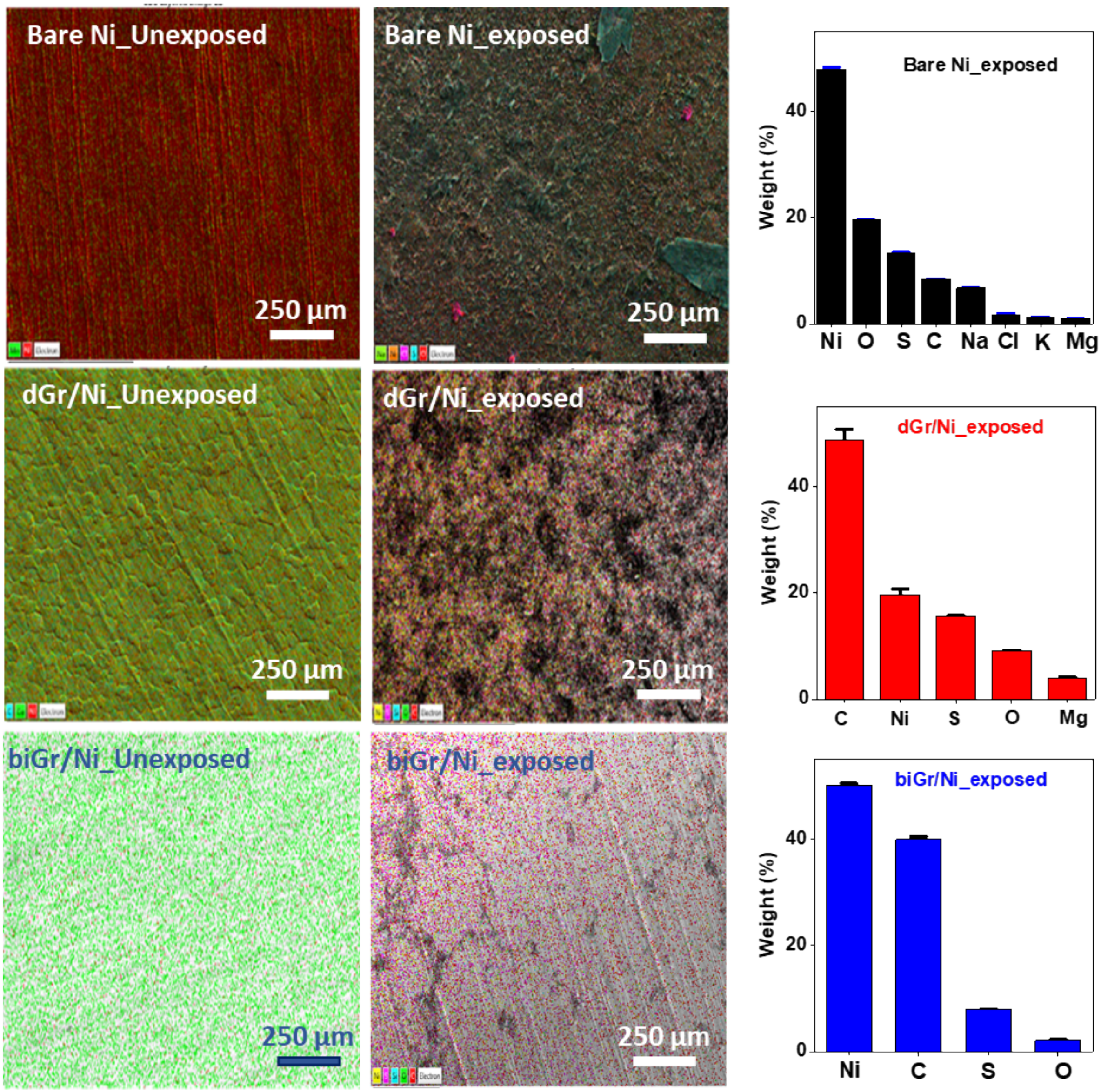

Figure S6. Energy dispersive spectroscopy on unexposed and exposed bare Ni, dGr/Ni, and biGr/Ni.

Surface morphology analysis of defect mediated abiotic corrosion: The dGr/Ni underwent greater attack than biGr/Ni (SEM images, Figure S5). The GB sites of dGr/Ni showed a strong preference to adhere salt (black patches, Figure S5e), which is similar to the preferential attachment of sessile OA-G20 cells in the GB region (Figure 4). The biGr/Ni was only slightly blemished by the percolation of electrolytes through the cracks in SS tests (Figure S5f). The tests based on SA also revealed intense attacks at the GB regions of dGr/Ni (Figure S5h) followed by the crumbling around the grain region. The stability of Gr coatings has been reported to be compromised by GBs due to their ability to promote uniform growth of the corrosive reactants.[16] Unlike bare Ni and dGr/Ni, the biGr/Ni experienced attack in the form of sporadic aggregation of Gr coating which is initiated through the cracks (Figure S5i).

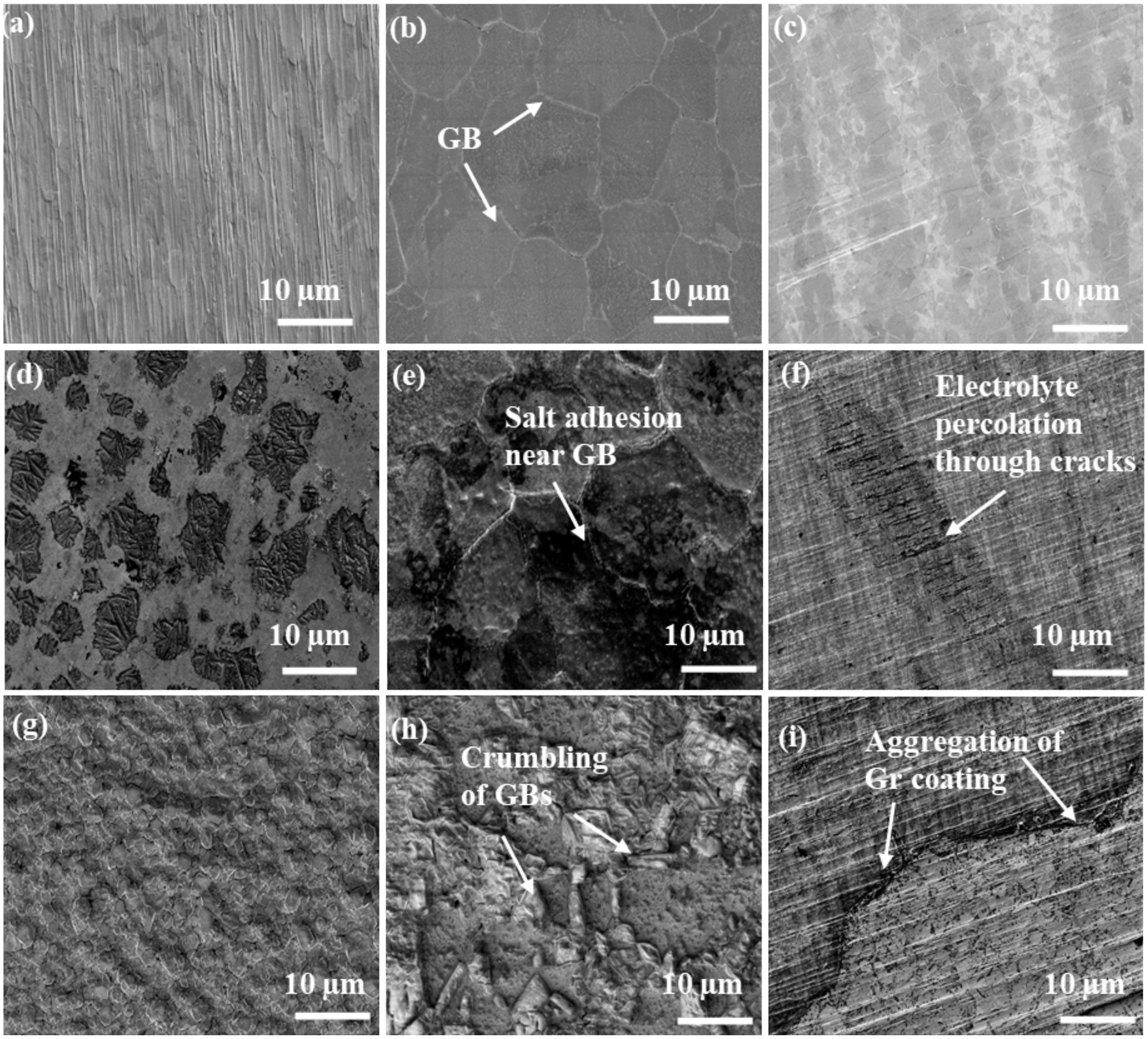

Figure S7. Defect mediated morphological features in abiotic environment. (a-c) SEM images of unexposed bare Ni, dGr/Ni, biGr/Ni, respectively. (d-f) SEM images of bare Ni, dGr/Ni, and biGr/Ni exposed to Na_2SO_4 solution, respectively. (g-i) SEM images of bare Ni, dGr/Ni and biGr/Ni exposed to H_2SO_4 solution, respectively. These images were taken with an excitation potential of 3.0 kV with 2468x magnification using the Everhart-Thornley detector (ETD).

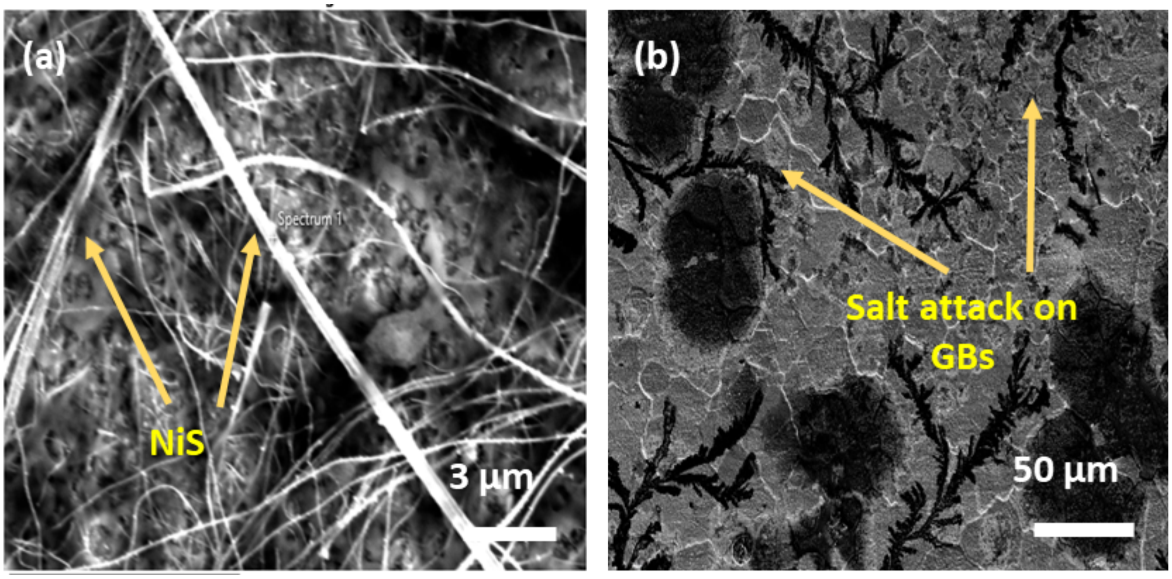

Figure S8. Morphological differences in biotic and abiotic exposure. (a) Elongated threads of biogenic sulfide formation observed in dGr/Ni surfaces (b) Intense salt attack along the GBs highlighted with dark patches and percolation

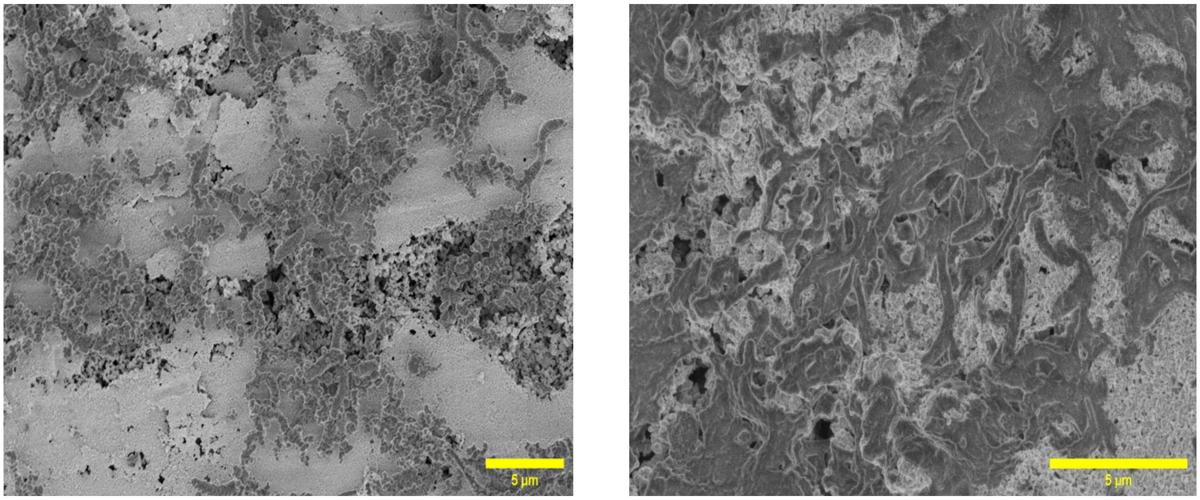

Figure S9. SEM image of Ni exposed to SRB. PMMA coated Ni (left) and bare Ni (right) showing insignificant difference in the bacterial adhesion between the two samples

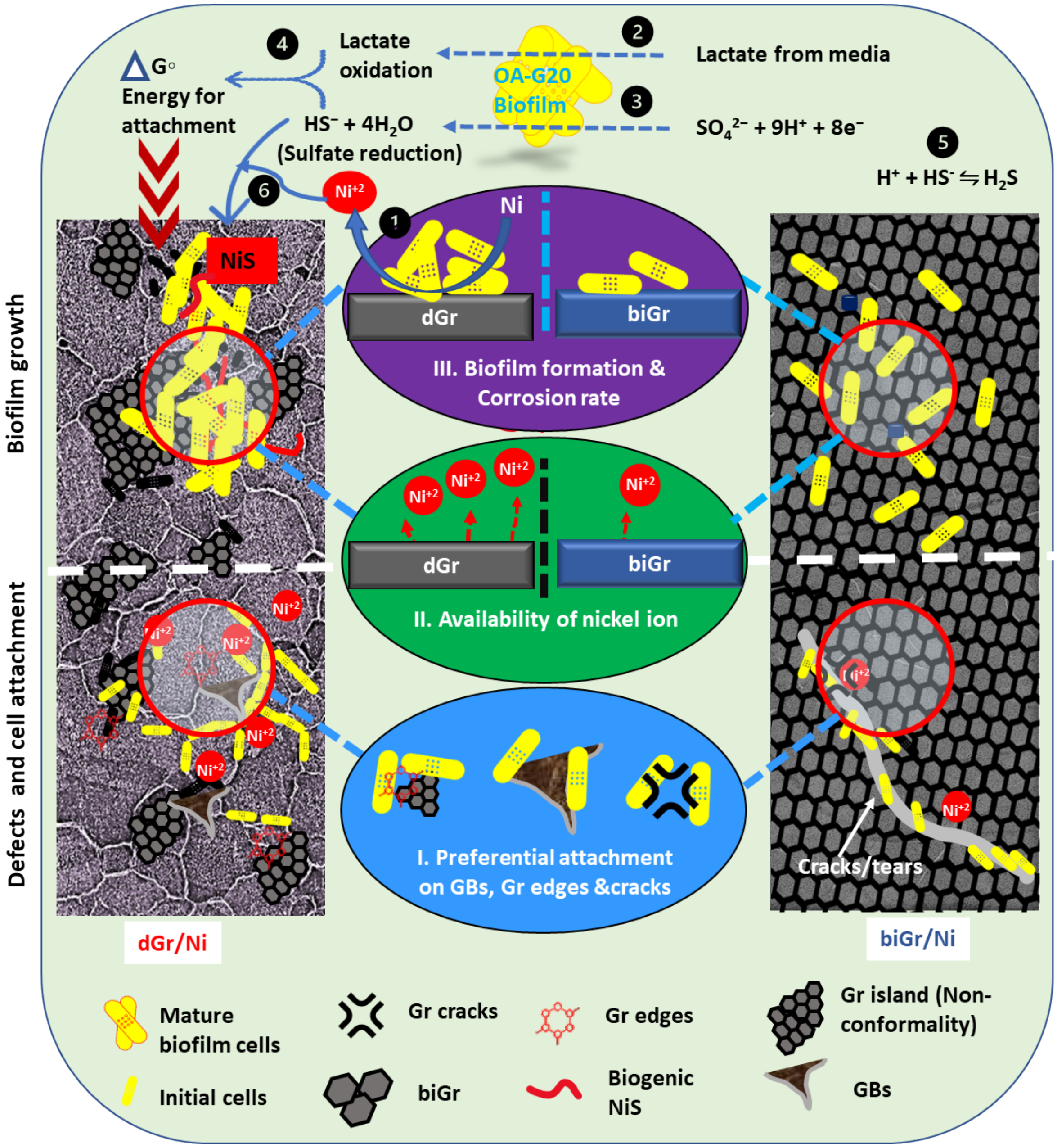

Figure S10. Effect of key defects on MIC performance of Gr/Ni. **Bottom panel:** Legends for OA-G20 cells, Gr coatings, and key defects including cracks, edges, islands, and grain boundaries (GBs). **Top Panel**: MIC Equations (1-6) shown as black circles. **Middle Panel**: Effects of the key defects under the following three categories *(I) Preferential attachment at the defective sites (blue oval) (II) Greater access to nickel ion (green) (III) Enhanced biofilm formation and corrosion (purple)*. Nonconformal Gr with reactive Gr edges and GBs (in dGr/Ni) accelerated preferential attachment of OA-G20 cells during the initial phase. Combined effects of the defects and increased cell attachment provided the OA-G20 cells on dGr/Ni with greater access to Ni^{+2} ions and promoted biofilm formation, while biGr/Ni acted as an impermeable barrier to resist Ni^{+2} dissolution and biofilm formation. The higher precipitation of accessible Ni^{+2} by OA-G20 caused ubiquitous presence of biogenic sulfide (NiS) on the dGr/Ni surface. The accumulation of NiS and the maturation of the biofilm accelerated increased MIC behavior of dGr/Ni compared to biGr/Ni and bare Ni.

References

[1] N. Yusof, B. Bais, N. Soin, B. Y. Majlis, *Wet Transfer Process for MEMS Freestanding PMMA/Graphene Membrane Development*, **2020**.

[2] M. S. Lee, K. J. Lee, *Hydrometallurgy* **2005**, *80*, 163. https://doi.org/10.1016/j.hydromet.2005.06.010.

[3] R. K. Sani, G. Geesey, B. M. Peyton, *Advances in Environmental Research* **2001**, *5*, 269. . https://doi.org/10.1016/S1093-0191(00)00061-7

[4] K. Jawaharraj, P. Sigdel, Z. Gu, G. Muthusamy, R. K. Sani, V. Gadhamshetty, *Environ Res* **2022**, *215*, DOI 10.1016/j.envres.2022.114045.

[5] G. Chilkoor, N. Shrestha, A. Kutana, M. Tripathi, F. C. Robles Hernández, B. I. Yakobson, M. Meyyappan, A. B. Dalton, P. M. Ajayan, M. M. Rahman, *ACS Nano* **2020**, *15*, 447. https://doi.org/10.1021/acsnano.0c03987.

[6] M. Pakiet, I. Kowalczyk, R. Leiva Garcia, R. Moorcroft, T. Nichol, T. Smith, R. Akid, B. Brycki, *Bioelectrochemistry* **2019**, *128*, 252. https://doi.org/10.1016/j.bioelechem.2019.04.005

[7] D. Parajuli, S. Sharma, H. B. Oli, D. S. Bohara, D. P. Bhattarai, A. P. Tiwari, A. P. Yadav, *Electrochem* **2022**, *3*, 416. https://doi.org/10.3390/electrochem3030029.

[8] A. A. Al-Amiery, A. B. Mohamad, A. A. H. Kadhum, L. M. Shaker, W. N. R. W. Isahak, M. S. Takriff, *Sci Rep* **2022**, *12*, DOI 10.1038/s41598-022-08146-8.